LAWRENCE
LIVERMORE
NATIONAL
LABORATORY

UCRL-JRNL-227058

Electrical and Optical Gain Lever Effects in InGaAs Double Quantum Well Diode Lasers

M. D. Pocha, L. L. Goddard, T. C. Bond, R. J. Nikolic, S. P. Vernon, J. S. Kallman, E. M. Behymer

January 4, 2007

IEEE Journal of Quantum Electronics

Electrical and Optical Gain Lever Effects in InGaAs Double Quantum Well Diode Lasers

Michael D. Pocha, *Senior Member, IEEE*, Lynford L. Goddard, *Member, IEEE*, Tiziana C. Bond, *Member, IEEE*, Rebecca J. Nikolić, *Member, IEEE*, Stephen P. Vernon, Jeffrey S. Kallman, and Elaine M. Behymer

***Abstract*— In multisection laser diodes, the amplitude or frequency modulation (AM or FM) efficiency can be improved using the gain lever effect. To study gain lever, InGaAs double quantum well (DQW) edge emitting lasers have been fabricated with integrated passive waveguides and dual sections providing a range of split ratios from 1:1 to 9:1. Both the electrical and the optical gain lever have been examined. An electrical gain lever with greater than 7 dB enhancement of AM efficiency was achieved within the range of appropriate DC biasing currents, but this gain dropped rapidly outside this range. We observed a 4 dB gain in the optical AM efficiency under non-ideal biasing conditions. This value agreed with the measured gain for the electrical AM efficiency under similar conditions. We also examined the gain lever effect under large signal modulation for digital logic switching applications. To get a useful gain lever for optical gain quenched logic, a long control section is needed to preserve the gain lever strength and a long interaction length between the input optical signal and the lasing field of the diode must be provided. The gain lever parameter space has been fully characterized and validated against numerical simulations of a semi-3D hybrid beam propagation method (BPM) model for the coupled electron-photon rate equation. We find that the optical gain lever can be treated using the electrical injection model, once the absorption in the sample is known.**

***Index Terms*— amplitude modulation, gain lever, photonic integrated circuits, semiconductor device measurement, semiconductor device simulation, semiconductor lasers**

I. Introduction

GAIN competition in lasers offers the potential of integrating several digital logic functions on the same chip and with many applications for all-optical, high-speed switching. Lasers with optical gain control, capable of routing and logic functions [1], [2] via the gain quench effect [3], [4] have been demonstrated. All-optical photonic integrated circuits where, edge emitting lasers and laser-logic (gain-quenched inverters & nor-gates) will be interconnected by passive waveguides in a monolithic integrated circuit are under investigation at LLNL. Gain in the active devices will be useful to overcome coupling and transmission losses in the passive waveguides. We are, therefore, investigating the gain lever effect to enhance the modulation efficiency of our active devices. Our test structures are InGaAs double quantum well (DQW) graded index separate confinement heterostructure (GRINSCH) lasers. The gain lever effect is illustrated in Fig. 1, where a cross-sectional schematic diagram of a split-electrode laser is shown, along with a representative gain curve. Lasing occurs when gain overcomes losses. The overall modal gain in a laser is clamped, in steady-state, approximately by the cavity losses. At the lasing threshold, an increase in gain in one section of the laser allows an equal decrease in gain of the other section ($\Delta G_a = \Delta G_b$ in the figure) and vice-versa. We call the shorter section *a* and the longer section *b*, the respective drive currents I_a and I_b and the respective current densities J_a and J_b. In the literature sections *a* and *b* are also referred to as control and slave sections, respectively. Section *b* is biased to a higher carrier density than section *a*. A small decrease in I_a reduces the carrier density in the section, reducing the total gain below the total loss. The circulating optical power decreases, which causes the carrier density of section *b* to increase. The carrier density continues increasing until the gain equal loss condition is re-established. However, due to the sub-linear gain versus carrier density relationship shown in the figure, the carrier density increase in section *b* is enhanced compared to the decrease in section *a*. The net result is an increase in the amplitude modulation (AM) efficiency, i.e. the slope efficiency of the laser.

The gain-lever effect has been extensively studied [5]–[13], especially in the context of electrical amplitude modulation in split electrode lasers. Vahala, Newkirk, and Chen [14] also show an optical gain lever in GRINSCH lasers. Most of these papers concentrate on the small signal behavior. Here, in addition to small signal behavior, we also study large signal modulation because our application is digital logic switching. We have conducted experiments and modeling to understand and optimize the gain lever effect. While ultimately interested in optical input, we began with electrical input to quickly verify our models before pursuing the more complex optical input study. Our numerical models [13] use a beam propagation method (BPM) that in combination with the

Manuscript received February 23, 2007. This work was performed under the auspices of the U.S. Department of Energy by University of California, Lawrence Livermore National Laboratory under Contract W-7405-Eng-48. UCRL-JRNL-227058

All authors are with the Lawrence Livermore National Laboratory, P.O. Box 808, L-222, Livermore, CA 94551-0808 USA (phone: 925-422-8664; fax: 925-422-2783; e-mail: pocha@llnl.gov).

method of characteristics greatly reduces the computational time and memory load. Experimentally, we fabricated a series of split electrode DQW lasers. We created 10%, 20%, 30%, 40%, and 50% electrode-length ratios of the shorter electrode to the total length of the lasing cavity. The gap between electrodes is 5 μm and the total length of our lasers is 300 μm. The laser width is 10 μm. We can independently apply current to the two sections of the laser and measure the optical power output as well as the voltage drop across the laser diode. The optical gain lever effect has also been investigated by illuminating the active layer in the gap between the split electrodes and by introducing pump light through localized holes etched in the metal and cladding layers using a focused ion beam (FIB) instrument.

II. Electrical Gain Lever Experiments

A. Test Devices

Our test devices use a standard DQW GRINSCH doping profile as shown in Table I. On an n+ GaAs substrate a 1.6 μm bottom cladding graded layer of AlGaAs is grown followed by two InGaAs quantum wells (each 11.5 nm thick with 15 nm spacing) and then a top cladding of 1.6 μm graded AlGaAs with a 0.2 μm GaAs cap. A standard ridge-waveguide index-guided laser is patterned with a ridge width of 10 μm. The laser wavelength varies from 950-970 nm depending on bias and temperature. The operation wavelength is close to 980 nm, but the In composition was slightly lowered since the accumulated strain would be too high given the desired QW thickness. A unique feature of our devices is that the facets are formed by etching vertical walls using an Electron Cyclotron Resonance (ECR) plasma etch process [15]. Fig. 2 is a plan-view photomicrograph of a typical split contact laser with the etched facet and the corresponding well in the GaAs formed by the etching process. In this figure, the laser waveguide is oriented vertically so that the light would exit the top and bottom of the photograph. The short electrode (section *a*) is at the bottom and the long electrode (section *b*) is at the top. The etched wells at the top and bottom of the laser create a region of free space to allow light to exit the chip. The simple sketch at right (not to scale) illustrates the physical structure.

A second unique feature of our devices is the incorporation of passive waveguides which will eventually guide light between active devices on photonic integrated circuits. Our approach to these passive waveguides is to deposit them within the etched wells using a photoresist lift-off process to self align the waveguide films with the etched wells. Currently, we are leaving the waveguides as broad area passive guides so that light is confined only vertically. We use an SiO_2-Ta_2O_5-SiO_2 dielectric structure for the passive waveguides [15].

B. Test Set-up

We make electrical and optical measurements using the system schematically shown in Fig. 3. LabView software is used to control the current sources and measure the resulting light power through a collection lens with numerical aperture (NA) of 0.85. The voltage is monitored so that a complete Light/Current/Voltage (*L*/*I*/*V*) set of data can be collected. Current source-1 has the capability to provide either pulsed or DC current, whereas Current source-2 provides only a DC bias. All measurements reported here are for DC current. The device under test is mounted in a temperature controlled probe station under a microscope. The microscope has a coaxial CCD camera to allow capture of images of the top of the device as it is being probed. Furthermore, the microscope has been modified to provide a second illumination path for a pump laser. The pump laser (Blue Sky Research FMXL-017, 635 nm, 17.5 mW max) can be modulated and the optical gain lever measurements presented in Section III use the lock-in amplifier to extract small AC signals on top of large DC powers. A standard silicon detector and optical power meter measure the test laser power at 950 nm. Filters placed in front of the detector are used to block scattered 635 nm pump light.

C. Gain-Lever Measurements

Gain-lever data are conventionally presented in one of two ways. One can plot optical power versus I_b with I_a stepped, see for example Seltzer *et al.* [11]. Alternately, Vahala *et al.* [14] plot change of output power versus change of input power (the optical equivalent of I_a) for different values of I_b. We use the latter approach as it allows a more direct measurement of the gain-lever. The gain-lever, *GL*, is defined as the internal differential conversion efficiency, η_c, i.e. the number of additional photons generated per input photon. When the two sections are shorted together, this conversion efficiency is unity [16] ($\eta_c^{shorted} = 1$). On a light versus current *L*/*I* plot, the measured slope efficiency above threshold represents the combined internal conversion and external extraction efficiency, η_{ce}. Using the result that $\eta_c^{shorted} = 1$, we can determine the gain-lever by calculating the ratio of the measured slopes:

$$GL \equiv \eta_c(J_a, J_b) = \frac{\eta_c(J_a, J_b)}{\eta_c^{shorted}} = \frac{\eta_{ce}(J_a, J_b)}{\eta_{ce}^{shorted}}. \qquad (1)$$

Note that we have assumed that the extraction efficiency is independent of biasing conditions. When the two electrodes are shorted together, current will distribute evenly along the length of the diode ($J_a = J_b$) and the laser is operated as if there is no split in the electrode. The slope efficiency of the device with electrodes shorted is the reference value (gain = 1) [11] because both sections of the laser are operating at the same bias point on the gain curve in Fig. 1. In all cases, we ignore the small perturbation in current flow that will occur under the gap between the electrodes. As an example, in Fig. 4, we plot the *L*/*I* curve for a typical split electrode device (L_a/L = 10%) with I_a along the bottom *x*-axis and single facet optical power along the *y*-axis. Since current density will be critical in the discussion of gain-lever that follows, the

secondary *x*-axis along the top shows J_a. Here, several curves with differing J_b bias are shown. The inset shows the single facet *L*/*I* curve for the shorted electrodes versus total current. By taking the ratio of the local slope at a point along an *L*/*I* curve to the slope of the shorted device, the gain lever can be calculated according to (1). In this example (see Fig. 4), this ratio is about 0.36/0.15 = 2.4 (≈ 3.8 dB) for the device biased at J_b = 1000 A/cm^2 and $J_a \approx 0$. We perform local smoothing of the curves before taking slopes of experimental data to reduce the inherent noise. The overall experimental error of *GL* is less than ±1 dB. For large signal modulation, the effective gain lever is calculated as the ratio of the slope of the secant between the two operating points to the slope for the shorted device.

Before discussing the more rigorous simulations in Section IV, it is instructive to describe the expected qualitative behavior and compare it to the measurements. Referring to Fig. 1, it is clear that when $J_a = J_b$, the two operating points are the same, therefore gain should be exactly 1 (0 dB). As J_a decreases from this operating point, gain steadily increases (as the slope gets steeper) until $J_a = 0$ or the laser stops lasing. For example, if absorption in section *a* exceeds gain in section *b*, the laser will stop lasing and the balance between loss and gain will no longer hold, resulting in low values for the slopes of the light-power vs. I_a curves. This can be seen in the lower end of the J_b = 750 A/cm^2 plot in Fig. 4. On the other hand if $J_a > J_b$, the operating points of the respective sections of the diode are reversed and a gain of less than 1 should be observed.

Small signal analysis of the coupled rate equations [16] predicts that the device experiences a maximum gain lever effect just above the lasing knee near threshold. As the circulating power increases, stimulated emission greatly decreases the long effective carrier lifetime in the control section, τ_a, but only slightly decreases the already short carrier lifetime in the slave section, τ_b. The strength of the gain lever, which is proportional to the ratio of these lifetimes, is reduced. Moreover, as the circulating DC photon density, S_{DC}, increases, the pinning of the carrier density in the control section becomes stronger and thus the section less able to respond to changes in I_a. Hence, the gain lever effect begins to saturate above the lasing knee [16]:

$$GL_0 = \frac{g_a'\tau_a}{g_b'\tau_b}\frac{1+v_g S_{DC} g_b'\tau_b}{1+v_g S_{DC} g_a'\tau_a}, \qquad (2)$$

where *g*' is the differential gain, v_g is the group velocity, and the subscript for GL_0 indicates that the result is valid only in the gain lever limit ($|L_aG_a/L_bG_b| << 1$). The saturation of the gain lever can be seen in Fig. 4 near $I_a = 0$, where the local slope decreases for increasing J_b above 1000 A/cm^2.

Several important features of the gain lever effect can be observed from the 2-D contour plot of Fig. 5, which shows the gain lever, *GL* (dB), versus both J_a and J_b for the L_a/L = 20% device. First, the operation point that has maximum *GL* is $J_a \approx 0$ and $J_b \approx 1000$ A/cm^2. This is expected since *GL* is strongest when J_a is minimum and the device is just above threshold Second, *GL* drops precipitously when the device drops below threshold as can be seen in the lower left corner of Fig. 5. Third, *GL* is zero within the experimental error of ±1 dB along the dotted $J_a = J_b$ line and moreover, the reverse gain-lever (*GL* < 0 dB) occurs above this line. Fourth, for fixed J_b (vertical slice), *GL* increases with decreasing J_a except if the laser drops below threshold. *GL* increases because operation point *a* in Fig. 1 moves to the left, which increases g_a'. Also, S_{DC} decreases and so *GL* is less saturated. Fifth, for fixed J_a (horizontal slice), *GL* increases with increasing J_b, except near threshold. Near threshold, S_{DC} increases rapidly and so the decrease in *GL* due to saturation outweighs the increase in *GL* as point *b* in Fig. 1 moves to the right. In contrast, far above threshold, S_{DC} does not increase as quickly and so the increase in *GL* from smaller g_b' becomes dominant. In summary, when the device is sufficiently above threshold, *GL* can be increased by decreasing J_a and/or increasing J_b.

In the gain lever limit or in the uniform injection limit ($J_a \approx J_b$), the predicted gain is independent of the split ratio. However, outside these limits, the non-negligible split ratio modifies (2) according to [16]:

$$GL = \frac{L_aG_a / L_bG_b + 1}{L_aG_a / L_bG_b + 1/GL_0}, \qquad (3)$$

Thus, if both sections are above transparency, the gain approaches unity (i.e. magnitude in dB decreases) for any fixed J_a and J_b as L_a increases, whereas it diverges away from unity (i.e. magnitude in dB increases) if one section is below transparency. To verify these conclusions, we have calculated the small signal gain, *GL*, for each split ratio and plotted this family of curves in Fig. 6 as a function of J_a with J_b fixed at 1000 A/cm^2. Since G_a is zero at transparency ($J_a \approx$ 400 A/cm^2), the laser will naturally be in the gain lever limit for any split ratio when section *a* is near transparency. The laser will be in the uniform injection limit when $J_a \approx J_b$. Thus, the devices should all behave qualitatively the same except when $J_a >> J_b$ or when $J_a \rightarrow 0$ and G_b is small compared to the unpumped absorption, $|G_a(J_a=0)|$ [16]. Fig. 6 shows that the curves do overlap to within the experimental error for most current densities despite the 5x variation in split ratio. At high J_a, the magnitude of the gain does appear to decrease as L_a increases, but the difference is comparable to the experimental error. We were unable to observe the dependence of the gain lever on the split ratio in the limit $J_a \rightarrow 0$ because the laser drops below threshold for L_a/L > 20%.

The effective gain lever for large signal modulation can be much smaller than for just above threshold small signal modulation because large signal modulation generates a large change in the two operation locations of Fig. 1. The reduction in the gain lever strength is quite visible in the data. In Fig. 4, the local slope decreases as I_a increases. This decreases the

slope of the secant line. In Figs. 5 and 6, the value for *GL* decreases as J_a increases, which also indicates a reduced gain for large signal modulation. To quantify the importance of this reduction, we calculated the effective gain for typical logic operations where the output power per facet is switched between 2.0 and 0.3 mW (just above threshold). For the device in Fig. 5 (L_a/L = 20%) biased at J_b = 1000 A/cm^2, the effective gain was 6.7 dB near threshold but only 2.7 dB as J_a switched between 870 A/cm^2 and 33 A/cm^2. At J_b = 750 A/cm^2, the effective gain was 1.3 dB near threshold but was -1.1 dB as J_a switched between 2200 A/cm^2 and 270 A/cm^2. The effective gain was negative for J_b = 750 A/cm^2 because most of the switching occurred under reverse gain-lever operation $J_a > J_b$. For the device with L_a/L = 40% biased at J_b = 2500 A/cm^2 (not shown), the gain was 7.4 dB near threshold and still remained high, 6.1 dB, as J_a switched between 333 A/cm^2 and 66 A/cm^2. We find that to achieve a fixed change in output power, a longer control section provides a better large signal gain lever because the control section remains closer to transparency, thereby maintaining the gain lever strength, and also because the slave section density can be higher at threshold, which increases the initial strength.

III. Optical Gain Lever Experiments

A. Test Devices

Optical gain lever measurements were made using the setup described earlier (Fig. 3). Our two contact devices have a window built-in (gap between electrodes), through which a small control section, comparable in size to the one used by Vahala *et al.* [14], can be illuminated. However, our region is not sufficiently isolated and carriers can easily diffuse into the gap and thereby reduce the strength of the gain lever. Also, without an electrical contact, we cannot measure the optical gain lever under various biasing conditions. We, therefore, make use of focused ion beam (FIB) etching to define carefully controlled windows through the metal and cap layers. At 635 nm, the pump light is far above the bandgap edge of the quantum well (QW) and of many of the GRIN and cap layers. Pump light will be absorbed in layers where the Al concentration is less than 41%. The absorption loss in the cap layers will substantially reduce the overall efficiency of light absorption in the GRIN and active layers. Thus, the FIB etch should be deep enough (> 0.5μm, i.e. midway into layer 13) to remove absorbing cap layers, but as shallow as possible to prevent optical loss for the circulating laser signal caused by damage to the GRINSCH waveguide. Examples of etched holes are illustrated in Fig. 7. Both one and two electrode lasers were etched. Despite removal of the cap layers, absorption of the surface normal pump light was quite small. About 5.6% of the light is absorbed in the GRINSCH and QW sections combined.

B. Test Set-up

The addition of the second illumination path in our probe station microscope has led to a number of concerns which need to be resolved to be able to make accurate measurements. Due to spherical and chromatic aberrations, there are noticeable differences in the focal plane location of the visible light illumination and the 635 nm pump. To determine the 635 nm focal plane, we used a procedure that first maximizes the open circuit voltage in the laser diode when optically pumped and then optimizes the focus by maximizing the modulation amplitude of the laser diode output power with J_b just above threshold. We measure the optical gain lever using small signal 1 kHz modulation of the 635 nm pump laser source and lock-in detection of the modulation in the 950 nm laser output. Two long pass filters remove the scattered pump light (≈ 1% of P_{in}) from the detected signal. Each filter begins to transmit light at 850 nm and has a 50 nm transition width. The combined filter suppression is over 50 dB at 635 nm. Thus, the scattered pump light that reaches the detector is less than $10^{-7}P_{in}$. The filter insertion loss at 950 nm is approximately 1 dB and collected data has been corrected for this loss.

C. Gain-Lever Measurements

Fig. 8 shows the small signal amplitude modulation at 950 nm from a single facet versus absorbed pump power at 635 nm for an unbiased control section (J_a = 0). The device under test is a 10x300 μm^2 two section laser with L_a/L = 10% (similar to device in Fig. 4). An 8x15 μm^2 window was etched with a FIB at the center of the control section for optical input. The curves are for different slave section biases, J_b, and corresponding DC output powers, P_{DC}. The threshold current density is $J_a = J_b$ = 750 A/cm^2 when shorted and J_b = 835 A/cm^2 when J_a = 0 A/cm^2. The optical pumping produced a linear response. We see no saturation effects with pump power because of the low input power (≈ 230 μW AC on a ≈ 230 μW DC bias), small absorption in the GRINSCH and QWs (5.6%), and wide total QW thickness (23 nm). The lock-in amplifier begins to lose its lock when P_{DC} exceeds about 1.2 mW, which corresponds to a DC to AC ratio of approximately 30 dB. This manifests itself as increased noise in the modulation response curves for J_b > 1000 A/cm^2. The cause of the loss of lock is unclear. We do not think it is a lock-in dynamic range issue because the analog to digital converter in the digital lock-in has 20 bit precision which implies that the ratio can be as high as 60 dB.

We do not see pure optical amplification, i.e. getting a larger output modulation signal than what was absorbed because of the low external differential quantum efficiency, η_e, of the lasers. The electrical L-I curve for the device had η_e = 21.5% from both facets. Thus, amplification from the optical gain lever effect will be masked by poor extraction efficiency of the laser signal. To investigate this further, we plotted the combined conversion and extraction efficiency from both facets for small signal optical and electrical modulation in Fig. 9. The electrical to optical conversion and extraction efficiency was obtained by directly measuring the *L*/*I* curve, whereas the optical to optical conversion (635nm to 950nm) and extraction efficiency used small signal lock-in

analysis. Lock-in data was discarded for $J_b > 1000$ A/cm^2 for $J_a = J_b$ because of the loss of signal locking above 1.2 mW. We derived the absorption of 5.6% by matching the optical and electrical combined conversion and extraction efficiency when the two sections are shorted together ($J_a = J_b$) and biased below threshold to avoid any saturation effects from circulating laser power. In other words, we are assuming that modulation in the sub-threshold output power is the same for an electrically injected electron-hole pair as an optically created pair. The agreement is quite good for a range of applied current densities below threshold. When $J_a = J_b$ and the device is above threshold, there appears to be a slight reduction in efficiency for optical pumping compared to electrical pumping. We believe that this is because the optical absorption in some layers for the 635 nm AC pump has been reduced by the optical pumping from the circulating 950 nm DC laser light. Specifically, the 950 nm light reduces the number of available electrons in the valence band that can be pumped by the 635 nm light and thus reduces the optical conversion efficiency above threshold.

Fig. 9 also shows experimental verification of the optical gain lever. For $J_b = 960$ A/cm^2, the combined conversion and extraction efficiency when the control section is unpumped ($J_a = 0$) is amplified by 2.5x or 4.0 dB relative to the uniformly pumped optical, and by 2.3x or 3.6 dB relative to the electrical case. The measured optical gain lever of 4.0 dB at $J_b = 930$ and 960 A/cm^2 is very close to the measured electrical gain lever of 3.8 dB for the $J_b = 1000$ A/cm^2 curve in Fig. 4. This is expected since the modulation efficiency should be independent of whether the carriers are electrically or optically injected. Also, just as in the electrical case, the device experiences a maximum gain lever just above the lasing knee. At medium operating currents, the optical conversion and extraction efficiency decrease to 35% and the shorted electrical efficiency asymptotes to 21%, yielding a decrease in the amplification from 2.3x or 3.6 dB to 1.67x or 2.2 dB. Far above threshold, the two curves will converge at 21% since the gain lever amplification decreases to unity according to (2).

IV. Theory and Comparison to Experiments

A. Numerical Model

Several models have been developed for analyzing laser nonlinear differential rate equations, but they are often reduced to a lumped parameter treatment or are implemented in the steady state rather than the transient regime, particularly in the case of optical gain lever [17]. Given the promise of gain lever technology, accurate time-domain (TD) modeling tools were developed for analysis and design [18], [19].

Here, we focus on our TD hybrid semi-3D model, solved using the effective index/beam propagation method with fast Fourier transform (EIM/BPM-FFT) in conjunction with the method of characteristics [20]. The model includes multiple controls, multiple wavelengths, gain saturation, a stochastic model of amplified spontaneous emission, and spatial hole burning, through carrier diffusion and multimode analysis.

After applying the effective index method (EIM) in the growth (y) direction, the slowly varying envelope approximation (SVEA), the method of characteristics, and the stochastic spontaneous emission source to the 3-D scalar wave equation, we obtain [19]:

$$\frac{\partial \Psi^{\pm}}{\partial z} = \pm \frac{1}{2ik_0 n_0}\left(\frac{\partial^2 \Psi^{\pm}}{\partial x^2} + k_0^2\left(n^2 - n_0^2\right)\psi^{\pm}\right) \pm \frac{n}{2n_0}\left(\frac{\Gamma g - \alpha}{2}\Psi^{\pm}\right) + \frac{1}{2n_0} S^{\pm}(x,z,t), \tag{4}$$

where $\Psi^{+}(x,z)$ and $\Psi^{-}(x,z)$ are the forward and backward electric fields, respectively, k_0 is the free-space wavenumber, n_0 and n are the background and modal refractive index, respectively, $(\Gamma g - \alpha)/2$ is the net modal gain for the electric field, g is the photon density (modal) gain, Γ is the vertical confinement factor, α is the distributed loss, and $S^{\pm}(x,z,t)$ represents the capturable spontaneous emission noise:

$$S^{\pm}(x,z,t) = \left(BN^2\right)\times \sum_{j=0}^{J-1}\sum_{l=0}^{L-1}\sum_{m=-M/2+1}^{M/2} \delta(t - j\Delta t)\times \left\{u\left[z-(l+1)\Delta z\right] - u\left(z - l\Delta z\right)\right\}\times \exp\left\{i\left[2\pi\left(mx/W\right) + \vartheta_{jl}^{m}\right]\right\}, \tag{5}$$

and is made up of M spatial sinusoids determined by total internal reflection (TIR). W is the laser width, u is the unit step function, and θ_{jl} are randomly generated phases at each step Δt and propagation $\Delta z = (cn_0/n^2)\,\Delta t$. The emission is scaled by the spontaneous emission rate (BN^2), $N(z,x,t)$ being the carrier density and B the spontaneous emission coefficient. By applying the FFT based BPM solver, one step advance yields:

$$\psi^{\pm}(x, z+\Delta z, t+\Delta t) = \exp\left[\mp\frac{i\Delta z}{2k_0 n_0}\frac{\partial^2}{\partial x^2} \mp \frac{ik_0\Delta z\left(n^2 - n_0^2\right)}{2n_0} \pm \frac{\Delta z\left(\Gamma g - \alpha\right)n}{4n_0}\right]\psi^{\pm}(x,z,t) + \Delta z S^{\pm}(x,z,t)/2n_0. \tag{6}$$

The first two terms of (6) are typical of the split-step approach since the first represents the propagation through a homogenous medium and the second gives the effect of a lens to account for the effective refractive index of the device. The index variation $n(N) = \alpha_{\varepsilon\nu}\, g(N)\, \lambda/(4\pi)$ is implemented here through the linewidth enhancement factor, $\alpha_{\varepsilon\nu}$.

The carrier density at every pixel in the (z, x) plane satisfies:

$$\frac{\partial N}{\partial t} = \frac{\eta_i J}{ed} - R(N) - \phi^{tot} v_g g(N) + D\frac{\partial^2 N}{\partial x^2}, \quad (7)$$

where η_i is the internal quantum efficiency, $J(z,x,t)$ is the applied current density, e is the electron charge, d is the thickness of the laser active area, $R(N) = AN + BN^2 + CN^3$ is the recombination rate, A and C are the defect and Auger recombination coefficients, respectively, $\phi^{tot} = \phi^+ + \phi^-$ is the total photon density, $\phi^{\pm}(z,x,t)$ are the forward (+) and backward (-) photon densities, respectively, and D is the diffusion coefficient. The material gain is modeled as:

$$g(N,\lambda,\phi) = \frac{g_0 \log(N/N_t)}{1+\varepsilon\phi^{tot}} \frac{1}{1+(\lambda-\lambda_0)^2/\Delta\lambda^2}, \quad (8)$$

where N_t is the transparency carrier density, ε is the saturation coefficient, and $\Delta\lambda$ is the Lorentzian spectrum's width [21].

B. Numerical Features

Our codes are written in Java and C++ to permit us to build and use a Graphical User Interface (GUI). The memory allocation is 40LM bytes, where L and M are the sampling points along z and x respectively, the run time is 15 min for LM = 3200 on a 1-GHz DEC Alpha. The numerical error is $O(\Delta z^3)$. The resolution usually used is L = 100 and M = 64. We typically also use a narrow super-gaussian as edge absorber. In Fig. 10, the evolution of the laser output originating from spontaneous emission is calculated. In the main plot area, the Fourier transform of the laser output over a local time window is shown at sampled time steps. The evolution of the random noise into selected longitudinal modes can be clearly observed as the laser light builds up from the beating of waves with time dependent random phases. A bandwidth of $\Delta\lambda$ = 5 nm was assumed for the lasers. The bottom plot of output emission power (split among the several longitudinal modes) as a function of time and shows relaxation oscillations. Final output power is approximately 10 mW.

C. Results and Comparisons

We applied our model to verify some of the trends observed in the measured gain-lever data. First, we replicated the shorted device using parameters extracted from our $L/I/V$ and spectrum measurements which yielded: η_i = 25%, loss α = 2 cm^{-1}, reflectivity R = 0.288, g_0 = 1900 cm^{-1}, N_t = 1.2x10^{18} cm^{-3}, λ_{peak} = 960 nm, $\Delta\lambda$ = 5 nm. Using our 1D solver (for the EIM approach) we derived the vertical overlap Γ_v = 0.072 ($\Gamma = \Gamma_v \Gamma_h$), the horizontal overlap is embedded in the solver. The other parameters A = 8x10^{-9} s^{-1}, B = 7x10^{-11} cm^3/s, C = 3.5x10^{-30} cm^6/s, D = 20.4 cm^2/s were derived from literature [21], [22]. The waveguide width used for the simulations was 10 μm. Fig. 11 presents a comparison of experimental results and simulations for (a) L_a/L = 10% (the device from Fig. 4) and for (b) L_a/L = 40%. The validation to the shorted LI curve is shown in the insets. In all cases, the data and simulations agree to within the experimental errors and device to device variation of about 0.5 mW.

Optical pumping can be approximately modeled using the electrical injection model. The absorbed power is converted into an appropriate injection current density. For our devices, the conversion is J_a = 0.056 P_{in}/(hνA) where A is the diode area, $h\nu$ is the pump photon energy in electron volts, and J_a is in mA for P_{in} in mW, since the absorption was 5.6%.

V. Conclusion

In conclusion, we have studied the gain-lever effect for an InGaAs DQW edge emitting laser. A small signal AM enhancement of 4 to > 7 dB for electrical modulation was measured near threshold for different split ratios L_a/L (from 10% to 50%). The AM gain for optical injection was similar under comparable biasing conditions. The gain is strongly dependent on the applied current density in the short contact J_a. The gain becomes negative (dB) when $J_a > J_b$ and sections a and b swap places on the material gain versus current density curve. For large signal modulation, the effective AM enhancement is reduced, especially in the short split ratio devices, because a sizable change in the control section carrier density is needed to achieve large output power switching. Nevertheless, an enhancement of 2.7 dB for L_a/L = 20% and 6.1 dB for L_a/L = 40% was achieved for a typical logic switching between 0.3 to 2.0 mW output power per facet.

Results were successfully compared and replicated with a hybrid semi-3D beam propagation code for several split ratios. Both electrical injection and optical pumping can be simulated with the same model.

The absorption for vertical pumping and the external extraction efficiency are too small for the optical gain lever to be useful in achieving optical transistor action in our current devices. Lasers with efficiencies over 60% are needed and in addition, a collinear or near collinear input will be required to increase the absorption length.

Acknowledgment

The authors would like to acknowledge the help of several of their colleagues in performing this work: Tim Graff, Jesse Wolfe, Paul Stratton, Warren Moberlychan, and Phil Stephan. We also wish to acknowledge useful discussions with Prof. Kerry Vahala at California Institute of Technology.

References

[1] A.B. Fowler, "Quenching of gallium-arsenide injection lasers," *Appl. Phys. Lett*, vol. 3, no. 1, pp. 1-3, July 1963.

[2] J.L. Fitz, W.T. Beard, S.C. Horst and S.D. Smith, "Integrated photonic inverter with gain," *IEEE Photon. Technol. Lett.*, vol. 13, no. 5, pp. 478-480, May 2001.

[3] H. Kawaguchi, *Bistabilities and Nonlinearities in Laser Diodes*, Boston MA, Artech, 1994, pp. 80-81

[4] W.J. Grande and C.L. Tang, "Semiconductor laser logic gate suitable for monolithic integration," *Appl. Phys. Lett.*, vol. 51, no. 22, pp. 1780-2, Nov. 1987.

[5] N. Moore and K.Y. Lau, "Ultrahigh efficiency microwave signal transmission using tandem-contact single quantum well GaAlAs lasers," *Appl. Phys. Lett.,* vol. 55, no. 10, pp. 936-938, Sept. 1989.
[6] D. Gajić and K.Y. Lau, "Intensity noise in the ultrahigh efficiency tandem-contact quantum well lasers," *Appl. Phys. Lett.,* vol. 57, no. 18, pp. 1837-1839, Oct. 1990.
[7] K.Y. Lau, "Frequency modulation and linewidth of gain-levered two-section single quantum well lasers," *Appl. Phys. Lett.,* vol. 57, no. 20, pp. 2068-2070, Nov. 1990.
[8] C.P. Seltzer, A.L. Burness, M. Stevenson, M.J. Harlow, D.M. Cooper, R.M. Redstall, and P.C. Spurdens, "Reliable 1.5 µm buried heterostructure, separate confinement, multiple quantum well (BH-SC-MQW) lasers entirely grown by metalorganic vapour-phase epitaxy (MOVPE)," *Electron. Lett.*, vol. 25, no. 21, pp. 1449-1451, Oct. 1989.
[9] C.P. Seltzer, L.D. Westbrook, and H.J. Wickes, "Improved signal-to-noise ratio in gain-levered InGaAs/InP MQW lasers," *Electron. Lett.*, vol. 29, no. 2, pp. 230-231, Jan. 1993.
[10] D. McDonald and R. F. O'Dowd, "'Inverted' gain-levered long-wavelength MQW optical transmitter with enhanced FM efficiency and suppressed AM," *Electon. Lett.*, vol. 30, no. 1, pp. 37-38, Jan. 1994.
[11] C. P. Seltzer, L. D. Westbrook, and H. J. Wickes, "The "gain-lever" effect in InGaAsP/InP multiple quantum well lasers," *IEEE J. Lightwave Technol.*, vol. 13, no. 2, pp. 283-289, Feb. 1995.
[12] J. Kuhn, B. Vollmer, A. Moritz, S. Heppel, C. Geng, F. Scholz, A. Hangleiter, and H. Schweizer, "Dynamic properties of GaInP multielectrode ridge-waveguide lasers," *Semicond. Sci. Technol.,* vol. 12, no. 4, pp. 439-442, Apr. 1997.
[13] M. Pocha, T. Bond, R. Welty, S. Vernon, J. Kallman, and E. Behymer, "Gain lever characterization in monolithically integrated diode lasers," in *Proc. SPIE*, vol. 5722, *Physics and Simulation of Optoelectronic Devices XIII*, *Photonics West Conf.*, San Jose, Jan. 2005, pp. 288-298.
[14] K.J. Vahala, M.A. Newkirk, and T.R. Chen, "The optical gain lever: A novel gain mechanism in the direct modulation of quantum well semiconductor lasers," *Appl. Phys. Lett.,* vol. 54, no. 25, pp. 2506-2508, Jun. 1989.
[15] R.J. Welty, T.C. Bond, E. Behymer, M. Pocha, G. Loomis, J. Wolfe, and S. Vernon, "Integrated laser with low-loss high index-contrast waveguides for OEICs," in *Proc. SPIE*, vol. 5729, *Optoelectronic Integrated Circuits VII*, *Photonics West Conf.*, San Jose, Jan. 2005, pp. 49-60.
[16] M.A. Newkirk, *Investigations of semiconductor laser modulation dynamics and field fluctuations,* Ph.D. dissertation, California Institute of Technology, 1991, Available: http://www.il.proquest.com.
[17] M.A. Parker and D.B. Shire, "A model for optically quenched lasers," *Appl. Phys. Lett.*, vol. 70, no. 2, pp. 146-148, Jan. 1997.
[18] T.C. Bond, J.S. Kallman, G.H. Khanaka, and M.D. Pocha, "Performance investigation of an all-optically controlled multi-section MQW laser for digital logic applications," in *OSA Annual Meeting Technical Digest*., Long Beach, Sept. 2001, p. 108.
[19] T.C. Bond and J.S. Kallman, "Time-domain tools for the investigation of gain-quenched laser logic," in *Proc. International Semiconductor Device Research Symposium,* Baltimore, Dec. 2003, pp. 506-507.
[20] M.D. Feit and J.A. Fleck, Jr., "Wave-optics description of laboratory soft-x-ray lasers," *J. Opt. Soc. Am. B*, vol. 7, no. 10, pp. 2048-2060, Oct. 1990.
[21] L.A. Coldren and S.W. Corzine, *Diode Laser and Photonic Integrated Circuits* (Wiley Series, 1995).
[22] J.-W. Lai and C.-F. Lin, "Carrier diffusion effect in tapered semiconductor-laser amplifier," *IEEE J. Quantum Electron*., vol. 34, no. 7, pp. 1247-1256, July 1998.

Michael D. Pocha (S'72, M'75, SM'99) received a B.S. degree from the University of California, Berkeley, in 1968, and M.S. and Ph.D. degrees from Stanford University, Stanford, California, in 1969 and 1976 respectively. From 1969 to 1971 he was a member of the Technical Staff of Bell Laboratories, where he worked on computerized fault diagnosis of digital circuits.

Since receiving his doctorate, he has been employed by Lawrence Livermore National Laboratory, where he has worked on a number of projects in the area of solid state devices and integrated circuits. Most recently, he has been concentrating on miniature optoelectronic sensor technology. He is currently the Chief Engineer of the Microtechnology Section of the Engineering Technologies Division. He has published over 40 papers in refereed journals and Conference digests and has been awarded several patents.

Dr. Pocha is a member of the Electrochemical society. He has won three R&D-100 awards given by R&D Magazine for the 100 most technologically significant products of each year.

Lynford L. Goddard (S'04, M'05) received the B.S. degree (with distinction) in math and physics, the M.S. degree in electrical engineering, and the Ph.D. degree in physics from Stanford University, in 1998, 2003, and 2005, respectively. His undergraduate honors thesis covered linear differential operators. At Xerox Palo Alto Research Center, he characterized the gain of 400 nm InGaN lasers during life testing. His doctoral research focused on characterization and modeling of 1.5-micron GaInNAsSb/GaAs lasers. He is currently a post doctoral researcher at Lawrence Livermore National Laboratory studying photonic integrated circuits. He is author or co-author of over 40 publications. Dr. Goddard is a member of the Optical Society of America and of the International Society for Optical Engineering (SPIE).

Tiziana C. Bond (S'91? M'96?) received the Laurea degree (cum laude) in electronic engineering from the University of Bari, Italy, in 1990 and the Ph.D. degree in electronic engineering from the Polytechnic of Bari, Italy, in 1995. Her doctoral dissertation was on a full vectorial finite element model for photonic devices. From 1995 to 1998, she held postdoctoral positions at the University of Florida and Georgia Institute of Technology working on Si-on-$LiNbO_3$ filters and polymer logic gates for optical communications.

In 1999, she joined Lawrence Livermore National Laboratory, as a Photonic Engineer, where she has worked on the development of integrated photonic platforms for all optical encryption circuits, miniature gas sensors, biological detection, and radiation diagnostic, in semiconductors and dielectrics. She has published over 30 papers. Dr. Bond is a member of the Optical Society of America. She was recipient of the Italian Department of Scientific Research Grant, the Italian Telecom Award, and the NATO Award.

Rebecca J. Nikolić (S'97, M'02), (previous publications under R.J. Welty), received the B.S. degree in Electrical Engineering from the University of California at Davis in 1997. In 1999, she received the M.S. degree and in 2002, the PhD degree in Electrical Engineering, specializing in Applied Physics, from the University of California at San Diego. Her dissertation research focused on the design, fabrication and characterization of high speed GaAs based HBTs. In 2002, she joined Lawrence Livermore National Laboratory as a Staff Research Engineer in the area of optoelectronic device development in the areas of secure communications and radiation detection. Her research interests include device physics, compound semiconductors and process technology development. She is author or co-author of over 30 publications. She is an elected Adcom member of the IEEE Electron Device Society.

Stephen P. Vernon received the B.A. degree in physics from the University of California at San Diego in 1973 and the M.S. and Ph.D. degrees in physics from the University of California at Santa Barbara in 1978 and 1980, respectively. He is a Staff Physicist at Lawrence Livermore National Laboratory. Prior to joining LLNL, he held positions as: an Independent Consultant in Applied Physics in Torrance, CA; a Senior Member of the Research Technical Staff at the Northrop Research and Technology Center, Palos Verdes, CA; a Staff Physicist at Energy Conversion Devices, Troy, MI; and a Visiting and Adjunct Assistant Professor within the Department of Physics at Arizona State University (ASU), Tempe, AZ; following post-doctoral appointments within the departments of physics at ASU and UCSB. His current research is focused on the development of photonics based, high-bandwidth radiation detectors. Previous research interests include low-defect deposition technology for fabrication of extreme ultra-violet lithograph (EUVL) masks, multilayer coating technology for EUVL optics, giant magneto-resistance multilayers for magnetic recording applications, and thin film synthesis. Dr. Vernon is a member of the OSA and the APS.

Jeffrey S. Kallman was born in Los Angeles, California in 1957. He obtained the B.S. degree in engineering from Harvey Mudd College in Claremont, California in 1979, the M.S. degree in electrical and biomedical engineering from Carnegie Mellon University in Pittsburgh, Pennsylvania in 1981, and the Ph.D. degree in engineering applied science from the University of California at Davis in 1994. He has worked at Lawrence Livermore National Laboratory as an Engineer since 1983. His current research interests are computational integrated photonics, inverse problems, and x-ray and ultrasonic imaging. Dr. Kallman was on the team that won an R&D 100 award for the MELD (Multiscale ELectroDynamics) simulation code in 1997.

Elaine M. Behymer has an AA degree in General Education and a certificate in Vacuum Technology from Chabot College. She joined Lawrence Livermore National Laboratory in 1978 and has 27 years of experience in semiconductor processing and working with silicon and III-V materials. Her expertise is semiconductor device fabrication equipment such as RIE, CVD, SEM, contact printing, magnetron sputtering, e-beam metal deposition systems, CAIBE, ozone, uv stabilization, HMDS oven, profilometers, diffusion furnaces, electro-plating, PECVD, nano-spec, RTA, and ECR etchers.

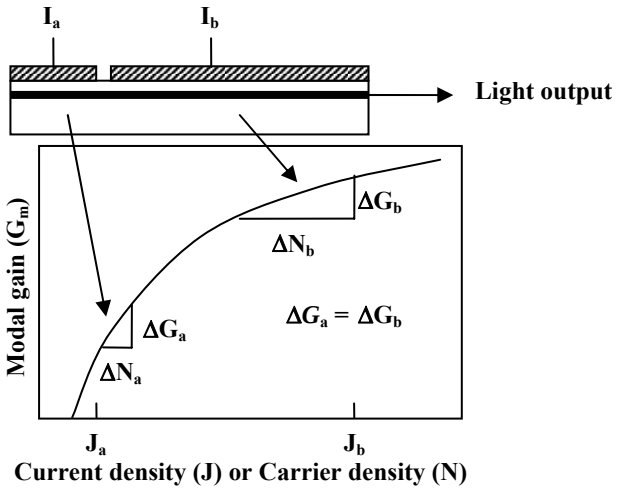

Fig. 1. The gain-lever effect**.**

Table I. Doping and thickness specifications of DQW epitaxial layer growth.

Layer #	Material Type	Alloy (x,y)	T (μm)	Doping (cm^{-3})	Type	Dopant
16	GaAs		0.02	1.6E+19	p+	Zn
15	GaAs		0.18	1.7E+18	p	Zn
14	Al(x)GaAs	0.2	0.2	2E+18	p	Zn
13	Al(x)GaAs	0.6->0.2	0.2	0.3->2E+18	p	Zn
12	Al(x)GaAs	0.6	1	2.8E+17	p	Zn
11	Al(x)GaAs	0.11->0.6	0.2	-	UD	-
10	Al(x)GaAs	0.11	0.01	-	UD	-
9	GaIn(y)As	0.11	~0.0115	-	UD	-
8	Al(x)GaAs	0.11	0.015	-	UD	-
7	GaIn(y)As	0.1	~0.0115	-	UD	-
6	Al(x)GaAs	0.11	0.01	-	UD	-
5	Al(x)GaAs	0.6->0.11	0.2	5E16->3E17	n	Si
4	Al(x)GaAs	0.6	1	2E+17	n	Si
3	Al(x)GaAs	0.2->0.6	0.2	2E17->2E18	n	Si
2	Al(x)GaAs	0.2	0.2	2E+18	n	Si
1	GaAs		0.25	2E+18	n	Si
	GaAs Substrate				n+	

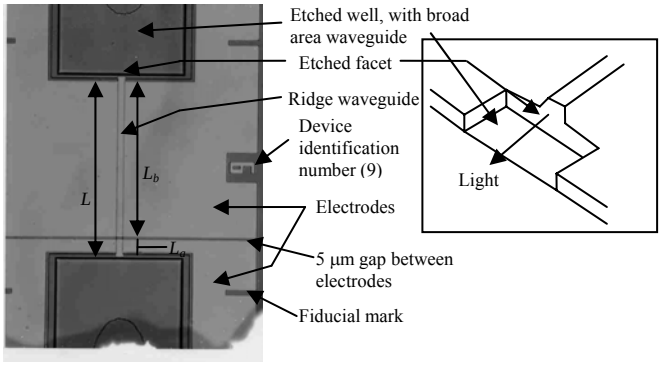

Fig. 2. Photomicrograph of a typical split-electrode laser.

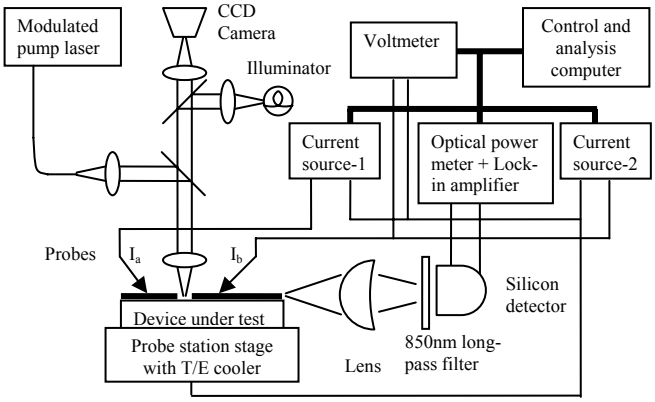

Fig. 3. Schematic diagram of test setup for probing and measurements of split-electrode lasers.

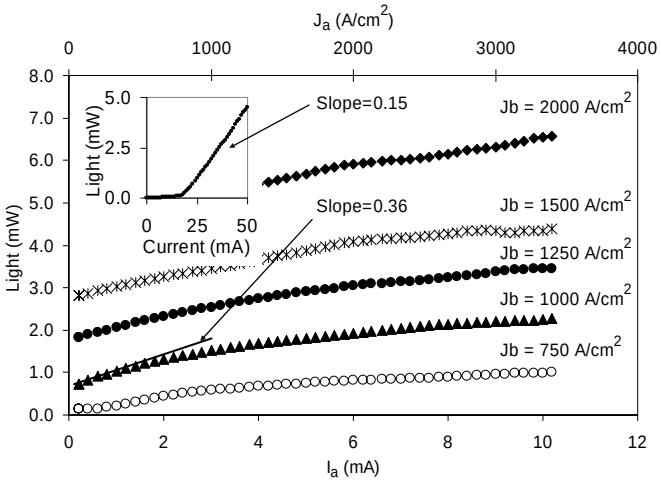

Fig. 4. Typical L/I_a curves for L_a/L = 10%. The gain lever, *GL*, is the ratio of the local slope to the slope of the *L*/*I* curve when the device is shorted (inset).

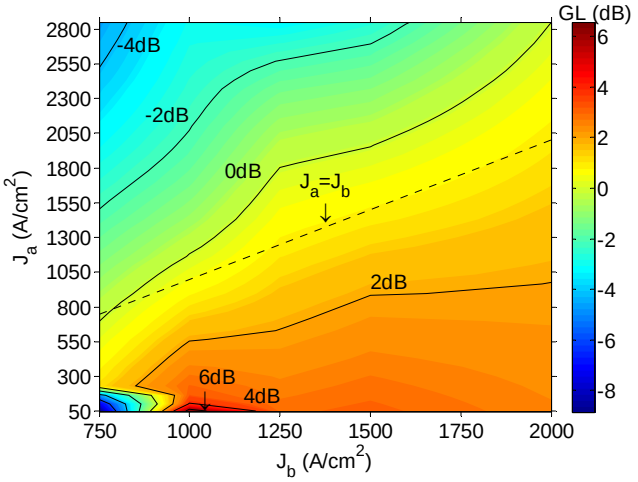

Fig. 5. Contour plot of the gain lever versus J_a and J_b for L_a/L = 20%.

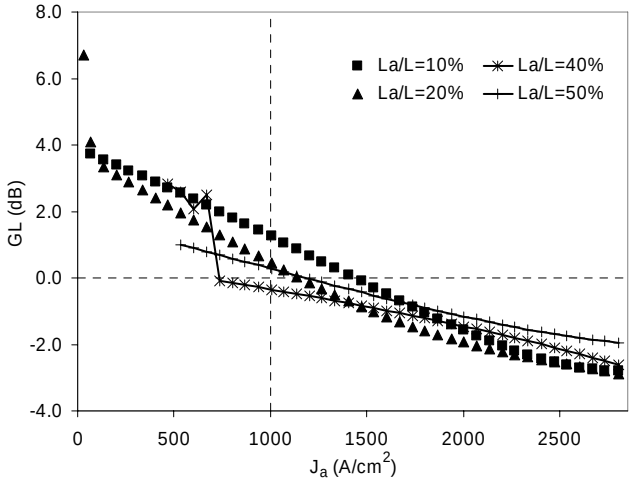

Fig. 6. Gain lever at J_b = 1000 A/cm^2 versus J_a for various split ratios. *GL* is positive for $J_a < J_b$ (upper left quadrant) and negative for $J_a > J_b$ (lower right).

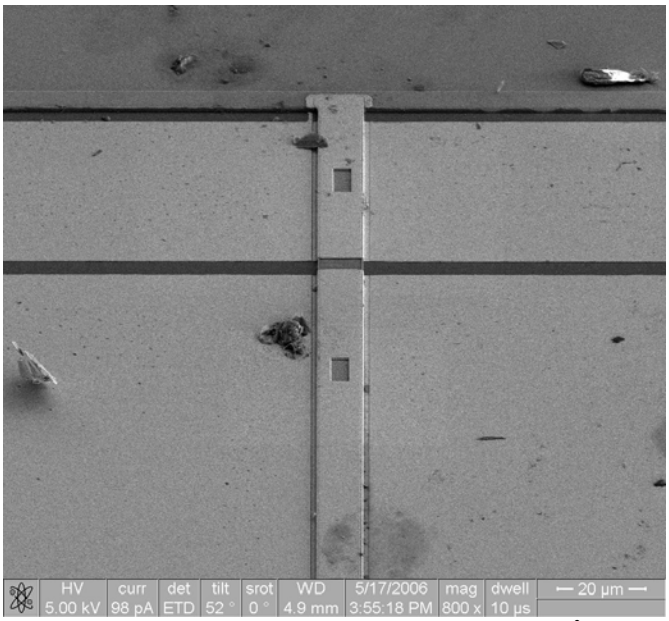

Fig. 7. SEM image of a 10 µm wide two section laser with 4x8 µm^2 FIB holes in the top control section (L_a = 30 µm) and bottom slave section (L_b = 270 µm). There is a 5 µm gap to separate the sections.

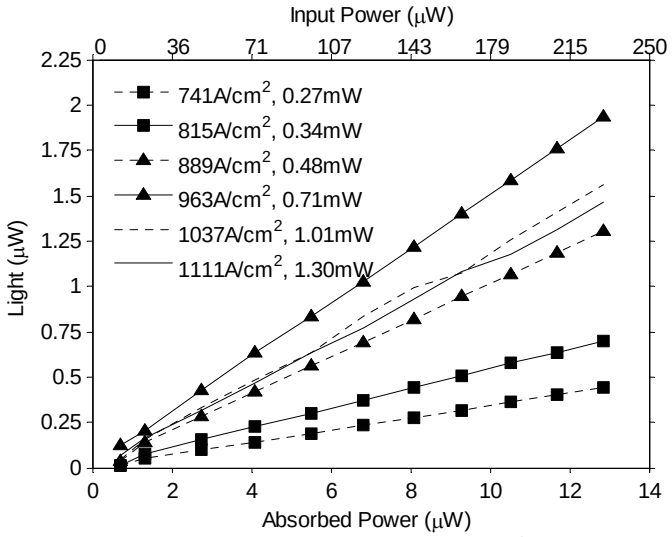

Fig. 8. Single facet output power at 950 nm for J_a = 0 A/cm^2 versus absorbed pump power at 635 nm (5.6% absorption). Legend gives values of J_b and P_{DC}.

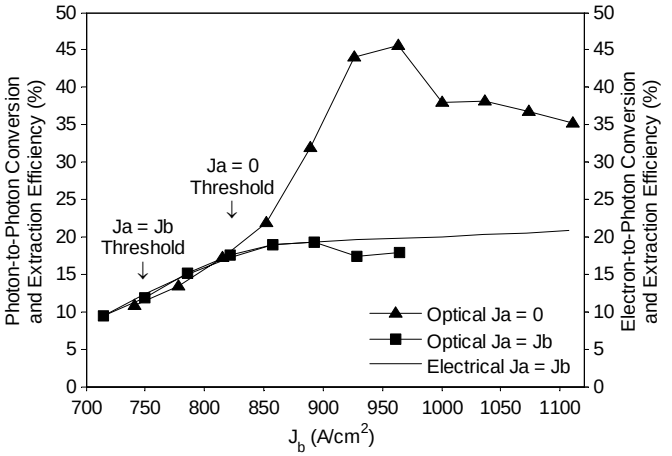

Fig. 9. Combined conversion and extraction efficiency from both facets for optical pumping (left axis) or electrical injection (right axis).

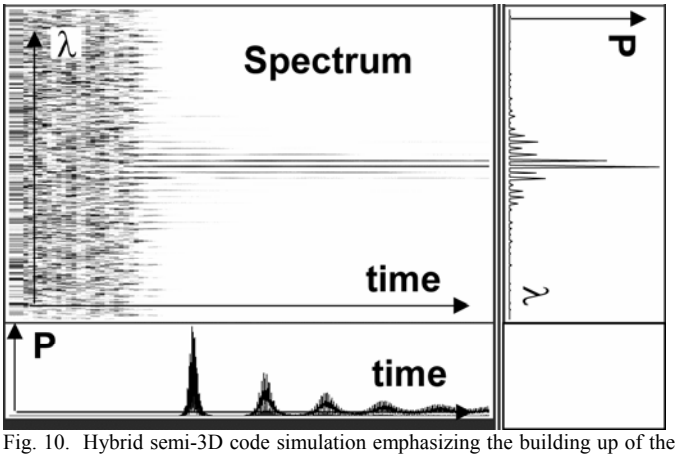

Fig. 10. Hybrid semi-3D code simulation emphasizing the building up of the laser output power and modes from amplified spontaneous emission.

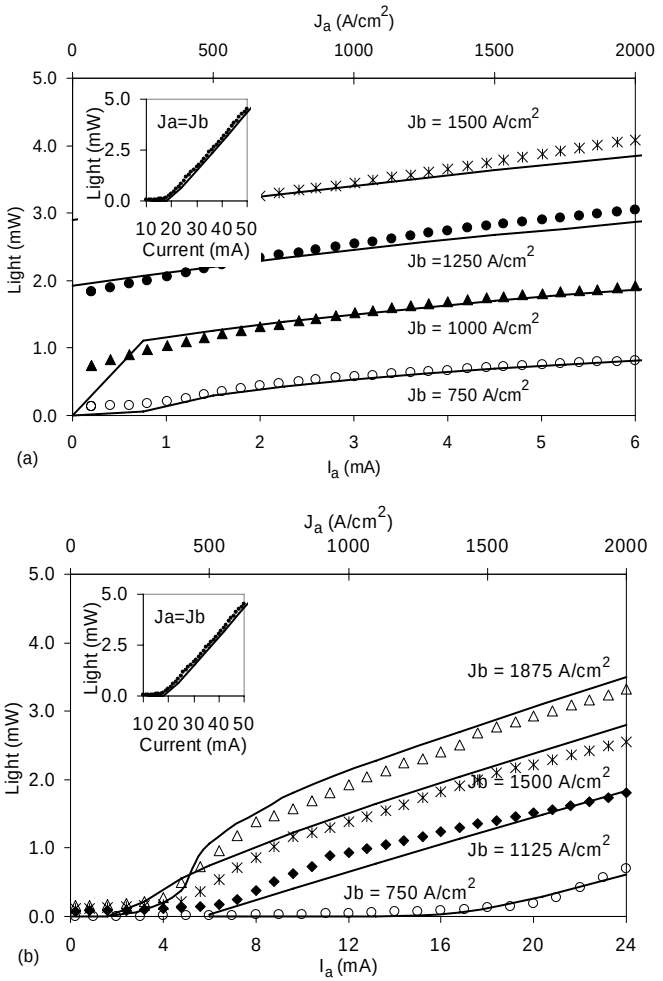

Fig. 11. Comparison of simulations (lines) and experimental results (points) for (a) L_o/L = 10% and (b) L_o/L = 40%. Insets show L/I curve comparison for shorted device.